Electrowetting of Hydrofluoroether Liquid Droplet at Gold Electrode/Water Interface: Significance of Lower Adhesion Energy and Static Friction Energy.

Tetsuro Morooka†, Takamasa Sagara‡,*

† Department of Advanced Technology and Science for Sustainable Development, Graduate School of Engineering, Nagasaki University, Bunkyo 1-14, Nagasaki 852-8521, Japan.

‡ Division of Chemistry and Materials Science, Graduate School of Engineering, Nagasaki University, Bunkyo 1-14, Nagasaki 852-8521, Japan.

E-mail: sagara@nagasaki-u.ac.jp

KEYWORDS Electrowetting, Hydrofluoroether, Interface, Au(1 1 1), Surface tension, Static friction energy, Adhesion energy

ABSTRACT: We explored the electrowetting behavior of a hydrofluoroester solvent, Novec 7100™ (Novec), as a liquid droplet on a Au(1 1 1) electrode in water (0.05 M $KClO_4$). Comparison with the electrowetting of hexadecane (HD) highlighted the significance of the lower adhesion energy and static friction energy of Novec than those of HD. The electrode potential-dependent contact angle θ of a Novec droplet showed little hysteresis. When potentials were set by means of potential steps, a Novec droplet increased its θ at more positive potentials than the potential of zero charge, pzc, of the Au(1 1 1) electrode. We found that the key factor of the electrowetting behavior for Novec is its low adhesion energy and static friction energy. The static friction energy of the oils to Au(1 1 1) electrode surface was evaluated by a comparative analysis of the potential dependence of the interfacial tension at the solid/water interface, $\Delta\gamma_{S/W}$–E curve, calculated from electrochemical surface charge data and the experimental $\cos\theta$–E curve; 2.6 mN/m for HD and 0.95 mN/m for Novec. When Br^- was added in the aqueous solution to allow its adsorption on the Au surface surrounding a Novec droplet, the potential of maximum $\cos\theta$ was shifted to negative. Overall, although the Novec droplet showed a narrower range of θ change than a HD droplet, the Novec droplet seldom got stuck to the surface as far as potential step was used, reflecting the narrower plateau region of θ near pzc. Also, the specific adsorption of a coexistent anion was a significant factor of θ. This work has featured the significance of a slippy droplet on an electrode surface, giving an impact on the technology of microfluid transportation control by electric potentials.

INTRODUCTION

The shape of a small droplet on a solid surface is determined by the balance of three interfacial tensions at each interface between two phases among the three[1]. The shape is represented by the contact angle, θ. The regulation technique of the shape change by electrical potential has been called electrowetting, which draws much attention to microfluidics[2-4]. Regulated changes of interfacial tensions can drive locomotion of the droplet on the solid surface. However, the methods for the locomotion are presently limited[5-13]. One way among them is a chemical modification of the surface to give an interfacial tension gradient. A directional gradient serves as a running track for a droplet. Typical methods to give the gradient on the solid substrate include surface functionalization by a self-assembled monolayer of amphiphilic molecules[5-10]. Another way is to introduce a local interfacial tension unbalance on the surface of a droplet put on the substrate by using adsorption-desorption of surfactants[11] or by light irradiation[12,13]. The local inhomogeneity of the surface tension causes a Marangoni effect and drives the deformation of the droplet. Therefore, the droplet shows spontaneous motion driven by the Marangoni effect, although the motion stops when an equilibrium reached.

Over the interfacial tension change by chemical modification or external stimuli, electrowetting has an advantage in faster and repeatable motion because of a quick dynamic decay of the electrochemical double layer structure to a new equilibrium upon potential change. In this paper, we consider key factors of an electrowetting system, especially the adhesion energy and static friction energy, keeping in mind that these are of profound importance in the droplet locomotion.

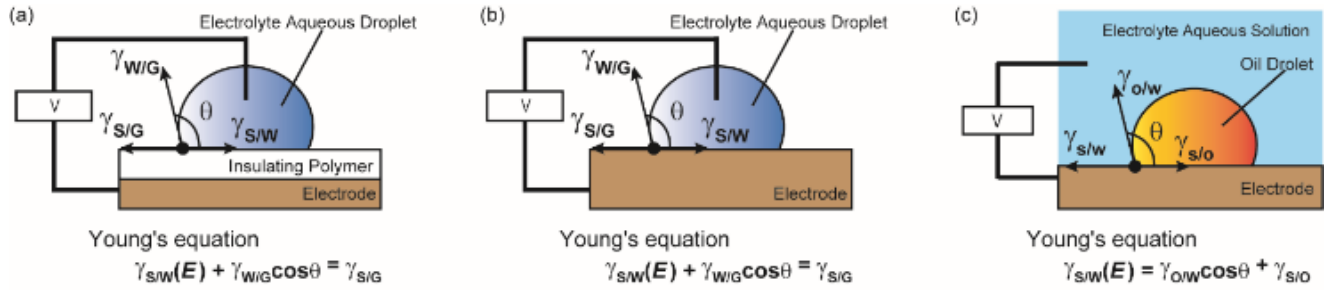

Figure 1. Typical configurations of electrowetting: (a) an electrolyte aqueous droplet in a gas phase (G) on an insulating polymer film on an electrode surface, (b) an electrolyte aqueous droplet in G directly on an electrode surface, and (c) an water-immiscible oil droplet in an electrolyte aqueous solution on an electrode surface. For each system, Young's equation is given with interfacial tensions, γ, and phase notations of water phase (W), solid substrate (S), and oil (O). Upon voltage application, only $\gamma_{S/W}$ is exclusively a subject of direct control.

Electrowetting on a dielectric (EWOD) is a technique of potential-dependent shape change of a droplet on a thin dielectric insulating underlayer. Usually, an electrolyte is dissolved in the droplet, in which one of the two electrodes is inserted, and the outer medium is a gas phase (Fig. 1–a). EWOD has been used in the microfluidic system or microreactor[14], although a high voltage is needed to give enough shape change to an aqueous electrolyte solution droplet placed on the air/insulated polymer coated electrode interface. Electrowetting has been frequently suffered from the saturation of θ. For example, when a high voltage over 100 V is applied, the θ of the droplet change becomes less than the theoretical value[3, 15–21]. Such a θ-saturation is caused by the polarization saturation of the insulated polymer surface or by non-linear electrode potential dependent of a charge density of the insulated polymer surface because of OH^- adsorption[20].

Electrowetting on a conductor (EWOC) has a direct contact of the electrolyte aqueous solution with the conductive electrode surface (Fig. 1–b and c). EWOC systems apply a voltage of 2 V or less, being much lower than the voltage for EWOD. For an EWOC system of an aqueous solution droplet on an electrode in air (Fig. 1–b with a counter electrode in the droplet) or an oil droplet on an electrode in an aqueous solution (Fig. 1–c with reference and counter electrodes in an aqueous medium), the potential dependence of the interfacial tension (γ) at the solid electrode/electrolyte aqueous solution (S/W) interface is the cornerstone of droplet shape regulation. The non-faradaic phenomenon that the interfacial tension at a S/W interface ($\gamma_{S/W}$) depends on the electrode potential is called electrocapillary, and it can control θ of a droplet repeatedly through the change of $\gamma_{S/W}$. The non-faradaic control of EWOC can be enhanced by potential-dependent intercalation or adsorption of anions at the S/W interface[22–25]. Faradaic processes have been used in some EWOC systems to achieve the locomotion of the droplet on the electrode surface. For example, Mukouyama and Shiono demonstrated a movement of a nitrobenzene droplet on a Au electrode in water in the same configuration as Fig. 1–c, where the interfacial tension change brought about by Sn electro-deposition on the Au electrode drives the movement[26]. A local unbalance of θ of the droplet originated from the fact that the interfacial tension increases with the Sn electro-deposition at one side of a droplet but decreases with the hydrogen generation at the opposite side. Arscott demonstrated a spontaneous movement of a HF aqueous solution droplet on the silicon wafer surface in air in the configuration of Fig. 1–b[27]. An inhomogeneous increase of θ is induced by a progressive chemical oxidation of H-terminated silicon surface by HF. Note that these redox-driven locomotions are not repeatable but have limited durability.

Regardless of which processes, non-faradaic or faradaic ones, are used, EWOC appears as a promising system to perform a locomotive droplet using the configuration of Fig. 1–c. There are, however, some drawbacks to drive the locomotion. The most serious one is the presence of plateau regions of θ, in which θ remains constant in an electrode potential region around the potential of zero charge (pzc)[23, 25, 28]. In these plateau regions, the adhesion energy W and the static friction energy F of a droplet limit its shape change. For the locomotion of a droplet by electrochemical control, our better choice is the oil that can exhibit smooth motion without getting stuck to the surface by a fine control of electrode potential. The adhesion energy W is defined as the work per a unit area required to detach an oil droplet (O) from a solid surface (S) in an aqueous medium (W), and it is given as the Dupré equation as[29]:

$$W = \gamma_{O/W} + \gamma_{S/W} - \gamma_{S/O} \quad (1)$$

Using the Young's equation representing a contact angle θ_t which is attained when any friction is not working:

$$\gamma_{S/W} = \gamma_{O/W}\cos\theta_t + \gamma_{S/O} \quad (2)$$

Eq. (1) can be rewritten as the Young-Dupré equation:

$$W = \gamma_{O/W}(1+\cos\theta_t) \quad (3)$$

When the contact area changes in the electrowetting behavior with the contribution of F, Eq. (2) should be modified, in order for the interfacial tension balance at the foot edge of an oil droplet at S/W interface to be considered[24], as

$$\gamma_{S/W} = \gamma_{O/W} \cos\theta_e + \gamma_{S/O} + F \quad (4)$$

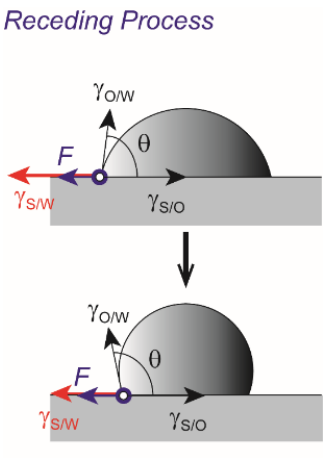

Figure 2. Droplet shape change with a contribution of a static friction energy F working in a receding process of electrowetting behavior.

where θ_e is an experimental value obtained by the contact angle measurements. F works in an opposite direction against the motion of the three-phase contact line in the electrowetting behavior as shown in Fig. 2.

Mertens and coworkers evaluated the changes of W and F for an aqueous electrolyte solution droplet on the electrode surface in air (configuration of Fig. 1–b)[24]. They used a boron nitride monolayer-modified Rh(1 1 1) electrode, where the hydrogen intercalation to the boron nitride layer takes place. They ascribed the changes to structure changes of the electrode surface with hydrogen intercalation.

The focus of this work is on the optimization of W and F to achieve more active EWOC in water giving smooth motion with insignificant plateau regions of θ at the electrode potentials around pzc. Because the origin of the plateau region has not been well understood, the clear solutions to the problem have not found. The aim of this work is at the quantitative evaluation of F and to provide a guideline to achieve plateau-less EWOC movements of an oil droplet. The guideline would serve as a basis of the techniques for realizing smooth on-surface locomotion of the droplet. To uncover the factors that limit the change of θ of an oil droplet, we compare the electrowetting behavior of a hydrofluoroether solvent Novec 7100™ (Novec) droplet with that of hexadecane (HD) droplet in water. In our previous paper[25], we studied the electrowetting of a HD droplet on a Au(1 1 1) electrode in water with concurrent specific adsorption Br^-. We found that the electrode potential dependence of θ of a HD droplet follows an electrocapillary equation. Specific adsorption of Br^- at the potential region between 0.0 V and +0.8 V as an atomic-level surface structural change of the electrode could be an additional driving force of the electrowetting, because the specific adsorption largely lowers $\gamma_{S/W}$. The specific adsorption causes a change of the surface charge density of the electrode and its potential dependence. As a result, the HD droplet is repelled from the surface at the potential region between 0.0 V and +0.8 V where the specific adsorption of Br^- anions takes place. We also found the appearance of plateau potential regions of θ for a HD droplet on the Au(1 1 1) electrode surface at the potentials both sides of pzc.

Referring to Eq. (3), W is greater with increasing $\cos\theta$ value and thus with wider spreading of the droplet. Therefore, an oil droplet with lower $\gamma_{O/W}$ attains more active and repeatable electrowetting at the S/W interface around $\theta \approx 90^\circ$ with narrower plateau regions.

Referring to Eq. (4), F represents the tendency of a droplet to resist the change of the contact area between an oil droplet and the electrode (O/W) surface in the electrowetting process. Again, a lower $\gamma_{O/W}$ is expected to show a shape change without both such plateau regions of θ and a hysteresis that a HD droplet showed.

In this study, we used a Novec droplet and explored its electrowetting on a Au(1 1 1) electrode. Using Novec as a liquid of low $\gamma_{O/W}$, we compared the $\theta - E$ (electrode potential) curve of Novec droplet with that of a HD droplet and discussed the effect of W and F on the electrowetting of the two liquid on the Au electrode surface. As a new approach, a theoretical electrocapillary curve was calculated from experimental surface charge–E curve and was compared with an experimental $\cos\theta - E$ curve to obtain F.

EXPERIMENTAL SECTION

Materials

The reagent grade HD was obtained from TCI. Novec 7100™ is a mixture of 95% n-$C_4F_9OCH_3$ (methyl nonafluorobutyl ether) and 5% i-$C_4F_9OCH_3$ (methyl nonafluoroisobutyl ether); we used this Novec from 3M Japan as obtained. Its properties are summarized in Table 1. Its solubility to water of 12 ppm (wt.) and water-solubility to Novec of 95 ppm (wt.) are also known[30]. Water was purified through a Milli-Q integral (Millipore) to a resistivity over 18 MΩ cm. Potassium perchlorate ($KClO_4$) of the highest reagent grade from Wako was recrystallized three times from water and was dried in vacuo. Ar gas was of 99.9995% purity. All other chemicals were of the highest reagent grade commercially available and were used as received.

A rod of cylindrical single crystal Au with a (1 1 1) surface base with an area of A = 0.272 cm^2 was purchased from Techno Chemics Inc. Immediately before its use as a working electrode, it was flame-annealed and quenched by water. A Ag/AgCl electrode in saturated KCl solution served as a reference electrode, and a coiled Au wire served as a counter electrode. The quality of the Au(1 1 1) electrode was examined by comparing its cyclic voltammogram (CV) and differential capacitance-potential (C–E)

curve in 50 mM $KClO_4$ solution with those in a previous report[31].

Table 1. Properties of HD and Novec.

	HD	Novec 7100™
$\gamma_{O/Air}$ (mN m^{-1})	27.6 [a]	10.1[f], 13.6 [f]
$\gamma_{O/water}$ (mN m^{-1})	53.3[b]	40
density (g mL^{-1})	0.77[c]	1.37[f]
viscosity (mN s^{-2} m^{-2})	3.591[d]	0.37[f]

a) from ref. 32, b) from ref. 33, c) from ref. 34 d) from ref. 35, and f) from ref. 36.

Electrochemical measurements

A quartz electrochemical cell was cleaned in a boiled sulfuric acid + nitric acid mixture and rinsed with a copious amount of purified water. The reference electrode was set in a separate compartment, which was connected to the main compartment through a liquid junction bridge. All the voltammetric measurement were made by setting the Au(1 1 1) electrode in a hanging-meniscus configuration to the electrolyte solution under a wetted Ar atmosphere in a Faraday cage at room temperature (22±2°C). We used 50 mM $KClO_4$ aqueous solution as the base solution.

A 1.0 μL droplet (< 3 mmϕ) was deposited on a Au(1 1 1) electrode surface using a procedure called Procedure B as described in our previous publication [25]; a 1.0 μL droplet was deposited using a micro syringe in air after a flame annealing treatment of the electrode.

Electrode potentials were controlled by a potentiostat (HUSO Electro Chemical System, HECS 9002) connected with a function generator. *C*-*E* curves were obtained from the ac voltammograms assuming an equivalent circuit of a capacitance of C and a resistance in series; C was equated to $[-2\pi f\,\mathrm{Im}(Z)]^{-1}$, where f = 14 Hz is the ac frequency of the ac potential modulation with an amplitude of 5 mV_{rms} and Im(Z) is the imaginary part of the ac impedance. For ac measurements, a lock-in amplifier (EG&G Instruments, model 7265) was employed.

A set of surface charge density (σ_M) -electrode potential (E) curves for a bare Au(1 1 1) electrode were obtained by potential step train chronoamperometry followed by current integration using the well-established protocol[37]. First, the initial potential E_i was applied. Then, the potential step was given to $E_f = \Delta E + E_i$. The potential step width, ΔE, may be positive to introduce adsorption process or negative to desorption process. The transient current was recorded as a function of time and integrated with respect to the time.

In situ contact angle measurements

For the measurements of θ_e of a 1.0 μL droplet in aqueous electrolyte solution, the image of the droplet on the electrode in the cell was captured by a digital microscope (J500-extreme). The obtained image was distorted by the curvature of the vertically-cylindrical electrochemical cell glass wall. The captured images were corrected in reference to a standard image of a perfect-sphere model ball lens (TECHSPEC N-BK7) of nearly the same size of the droplet to evaluate θ_e; the correction was to compress the horizontal lengths in the images by ×0.78 (Figure S1-a). The value of θ_e of the liquid droplet was evaluated graphically as shown in Figure S1-b. Note that, as described in our previous publication[25], because the droplet diameter in this study was always smaller than the capillary length (1.8 mm)[38], the gravity affects the shape of a smaller droplet negligibly.

RESULTS AND DISCUSSION

Electrowetting: HD on Au(1 1 1) electrode

First, we will show the fact that rather the large adhesion energy W and the static friction energy F limit the electrowetting behavior of a HD droplet on a Au(1 1 1) electrode around pzc. This fact will be the basis of our comparison of electrowetting behavior between Novec and HD as well as the discussion on the effect of W and F in section 3.2.

Recall that, in the Young's equation (Eq. 2), the value of θ_t is a theoretical value that can be experimentally realized only when F = 0. Because $\gamma_{O/W}$ and $\gamma_{S/O}$ are potential-independent constants in our system, $\gamma_{S/W}$ is linear to $\cos\theta_t$. This relationship is observable when the interfacial tension balance establishes an equilibrium without any hysteresis. In such a case, the potential-dependent dynamics of $\gamma_{S/W}$ could be observed as a time-change of $\cos\theta_e$ approaching to $\cos\theta_t$. Using constants of a and b, if $\cos\theta_e$ differs little from $\cos\theta_t$, we can write

$$\cos\theta_e = a\,\gamma_{S/W}(E) + b \qquad (5)$$

Eq. (5) demonstrates that $\cos\theta_e$–E plot should have almost the same curve shape as a $\gamma_{S/W}$–E plot, the electrocapillary curve. When $\theta_e = \theta_t$, the constant a corresponds to $1/\gamma_{O/W}$ and b does to $-\gamma_{S/O}/\gamma_{O/W}$. Note that $\gamma_{S/W}$ and $\gamma_{S/O}$ are not directly measurable at a solid electrode. The electrocapillary equation describes $\gamma_{S/W}$ on an electrode surface as[39]:

$$-\mathrm{d}\gamma_{S/W} = \sigma_M \mathrm{d}E \qquad (6)$$

where E is the electrode potential in reference to the pzc. In general, a σ_M–E curve is obtained from a potential step train chronoamperometric measurement as mentioned in the experimental section. Once σ_M–E curve is obtained, Eq. (6) permits us to obtain $\Delta\gamma_{S/W}$–E curve by the integration of σ_M–E curve with respect to E, where $\Delta\gamma_{S/W}$ is the relative value of $\gamma_{S/W}$ with respect to that at a base potential. The obtained $\Delta\gamma_{S/W}$–E curve is regarded as a theoretical $\cos\theta_t$–E curve. The electrocapillary curve ($\Delta\gamma_{S/W}$–E plot) shows a shape of an inverted parabola as a whole as a function of the electrode potential when no adsorption of solute takes place. The potential of σ_M = 0 is the potential of zero charge

(pzc), and $\Delta\gamma_{S/W}$ takes maximum at pzc (+0.23 V for bare Au(1 1 1) electrode in 50 mM $KClO_4$ aqueous solution).

As shown in Eq. (3), W steeply increases when the droplet spread wider through $\cos\theta_e \approx 0$. In addition, the droplet is difficult to change its shape if F works. F appears as a mechanical factor to limit the electrowetting as shown in Eq. (4). On the basis of this, comparison between the experimental $\cos\theta_e$–E curve and the $\cos\theta$–E curve (the $\Delta\gamma_{S/W}$–E curve which is theoretical value of integrated σ_M–E curve of the bare Au(1 1 1) electrode in the potential step chronoamperometric measurements) should uncover the effect of F on the electrowetting behavior.

The values of σ_M and θ_e at a given potential are sensitive to the surface condition such as surface reconstruction structures. The value of $\cos\theta_e$ of a HD droplet at the S/W interface is determined by the balance of the interfacial tensions at a three-phases contact line. Among them, $\gamma_{S/M}$ is the same as that at the surface area away from the contact line. Therefore, we use the value of σ_M of the bare electrode without oil droplet. An essential variable describing S/W interface is the surface charge density, σ_M. Therefore, we proposed to describe θ as a function of σ_M of the bare Au(1 1 1) electrode instead of as a function of the electrode potential[25].

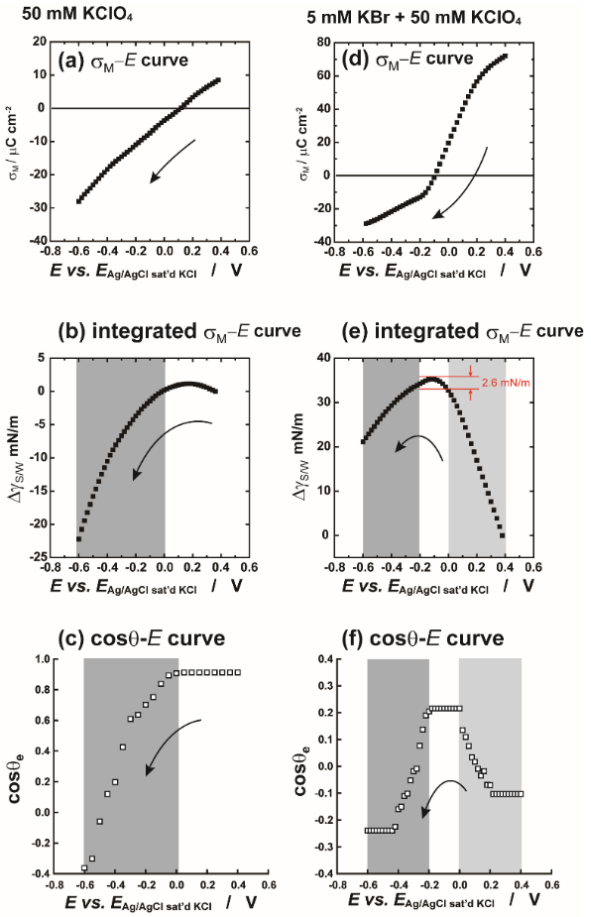

Figure 3. (a) σ_M–E curve of bare Au(1 1 1) electrode in 50 mM $KClO_4$ aqueous solution. (b) $\Delta\gamma_{S/W}$–E curve calculated from σ_M–E curve given in (a). Each value was integrated from the initial potential +0.40 V. (c) Experimental $\cos\theta_e$–E curve of HD 1.0 μL droplet on Au(1 1 1) electrode surface in $KClO_4$ aqueous solution. (d) σ_M–E curve of bare Au(1 1 1) electrode in 5.0 mM KBr + 50 mM $KClO_4$ aqueous solution. (e) $\cos\theta_e$–E curve; theoretical $\Delta\gamma_{S/W}$–E curve calculated from σ_M–E curve (d). Each value was integrated from the initial potential +0.40 V. (f) Experimental $\cos\theta_e$–E curve of HD 1.0 μL droplet on Au(1 1 1) electrode surface in KBr + $KClO_4$ aqueous solution. The experimental data (a), (c), (d) and (f) were obtained in negative potential step measurements; the initial potential (E_i) was fixed at +0.40 V to obtain the data points of negative-going to –0.60 V as final potentials (E_f).

In Fig. 3, the σ_M–E curves were obtained at a bare Au(1 1 1) electrode in $KClO_4$ aqueous solution (Fig. 3–a) or KBr (5 mM) + $KClO_4$ solution (Fig. 3–d) in negative potential step measurements in the absence of HD. The $\Delta\gamma_{S/W}$–E curves (Fig. 3–b and e) were calculated from these σ_M–E curves (Fig. 3–a and d, respectively). The $\cos\theta_e$–E curves of a HD 1.0 μL droplet on the Au(1 1 1) electrode surface in $KClO_4$ aqueous solution (Fig. 3–c) or KBr + $KClO_4$ solution (Fig. 3–f) were measured by negative potential steps. Integration of σ_M–E curves to obtain $\Delta\gamma_{S/W}$–E curves were made by setting the initial potential +0.40 V.

The plateau regions were observed from 0.00 V to +0.40 V in $KClO_4$ solution (Fig. 3–c) and from –0.22 V to 0.00 V in KBr + $KClO_4$ solution (Fig. 3–f). In these regions, the droplet showed the widest spreading so that $\cos\theta_e$ and W showed the greater values than those at other potentials. As shown in Fig. 2, when the difference between $\gamma_{S/W}$ and $\gamma_{S/O}$ reaches the maximum value of F, the droplet begins to change its shape in electrowetting. The smaller value of $\cos\theta_e$ than $\cos\theta_t$ is caused by F. Therefore, F reflects in the difference of the appearance of plateau regions in between $\Delta\gamma_{S/W}$–E curve and $\cos\theta_e$–E curve. Taking a close look at the $\Delta\gamma_{S/W}$–E curve in the plateau potential range of $\cos\theta_e$, we found that the greatest span of the $\Delta\gamma_{S/W}$ change therein was 1.2 mN/m in Fig. 3–b and 2.6 mN/m in Fig. 3–e. It turns out that the value of F working in the potential region E > pzc is 2.6 mN/m at a maximum in KBr solution. In other words, the change of $\Delta\gamma_{S/W}$ needs over 2.6 mN/m to show the shape change of the HD droplet on the Au(1 1 1) surface.

Electrowetting: Novec on Au(1 1 1) electrode

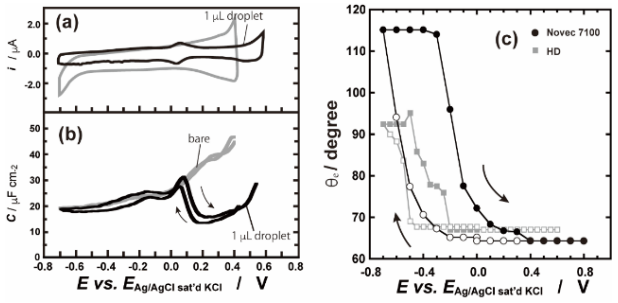

Figure 4. Voltammograms for a Novec 1.0 μL droplet-attached Au(1 1 1) electrode in 50 mM $KClO_4$ aqueous solution: (a) CV at a potential sweep rate of 20 mV s^{-1}, (b) *C*–*E* curve at a sweep rate of 5 mV s^{-1}. The gray lines in (a) and (b) were obtained for a bare Au(1 1 1) electrode without HD. (c) θ_e–*E* curve obtained by potential sweep method at v = 10 mV s^{-1}.

In previous section, *F* is evaluated for HD on a Au(1 1 1) surface to be 2.6 mN/m. The value of *W* is largely determined by $\gamma_{O/W}$ so that *W* at a given θ_e for Novec will smaller than that of HD. This estimation promises a narrower plateau region of θ_e for a Novec droplet at positive potentials to pzc than that of a HD droplet.

In this section, we describe an electrowetting behavior of a Novec droplet to experimentally uncover the effect of its lower *W* to Au(1 1 1) electrode surface. Fig. 4 shows typical CV, *C*–*E* curve, and θ_e–*E* curve for a 1.0 μL droplet of Novec in 50 mM $KClO_4$ aqueous solution. Both CV and *C*-*E* curve (Figs. 4–a and 4–b) were measured by setting an initial potential at +0.6 V. In Fig. 4–c, θ_e was tracked by scanning 0.0 V → –0.7 V → +0.7 V → 0.0 V. An appearance of a couple of CV peaks around +0.07 V (Fig. 4-a) and a change of the capacitance level in the range of 0.00 V to 0.14 V (Fig. 4–b) are of the same features as that we observed for a 1.0 μL droplet of HD (Fig. 1-a in our previous paper[25]). The appearance of low capacitance regions in both CV and *C*–*E* curve is indicative of the formation of Novec microdroplets around the 1.0 μL droplet. The electrode surface area covered by the 1.0 μL droplet, which was ca. 10% at the potential between +0.10 V and +0.70 V, was much less than the covering area of ca. 75% as calculated from the decrease of the differential capacitance. The presence of many tiny microdroplets forming around the 1.0 μL droplet resolves this discrepancy. It has been also the case for HD a 1.0 μL droplets, and the presence of HD microdroplets was confirmed by the fluorescence microscopy[25]. Upon immersion of the electrode with a hanging droplet of HD and Novec in water from a gas phase, the contact area of the droplet to the electrode surface largely decreases; this movement of the 1.0 μL droplet leaves a number of microdroplets. For both Novec and HD, such microdroplets dominate the electrochemical responses. These microdroplets were formed in the process that a 1.0 μL droplet put on the electrode in air was brought into contact with the aqueous electrolyte solution. Because the interfacial tension at Novec/water interface (40.0 mN/m as we measured using the Wilhelmy plate method) is larger than the interfacial tension at Novec/air interface (10.1 mN/m), a Novec droplet repels the surface, and these microdroplets remain at the S/W interface. As mentioned in our previous paper[25], these microdroplets are exclusively found in the Au/solution interface portion that has never been swept by the 1.0 μL droplet under potential control. These microdroplets hardly coalesce with the 1.0 μL droplet and never affect the potential-dependent shape change of the 1.0 μL droplet.

The initial value of θ_e of Novec at 0.00 V before the potential sweeping (64°) was smaller than the value of θ_e of a HD droplet (67°), because the interfacial tension at Novec/water interface (40.0 mN/m) is smaller than the interfacial tension at HD/water interface (53.3 mN/m). When sweeping the potential from 0.00 V to negative, the value of θ_e of a Novec 1.0 μL droplet began to increase from 65° at −0.30 V to 115° at −0.70 V (Fig. 4–c). After the turning of the potential scan to positive, the decrease in θ_e occurred between –0.30 V and +0.40 V. At the negative potential region, the greater θ_e change (from 65° at –0.30 V to 115° at –0.70 V) was observed for Novec than for HD. The smaller $\gamma_{O/W}$ value for Novec than that for HD causes a greater change of θ_e, because such a change is needed to balance with $\gamma_{S/O}$ and $\gamma_{S/W}$. The hysteresis in the negative potential region was of a greater extent for Novec than for HD. This hysteresis is caused by *F*, because the both shape-change processes of repelling and spreading take place in opposite direction to each other. Thus, the hysteresis width of θ_e reflected excess surface energy equivalent to 2*F*. In addition, the hysteresis width may be apparently enlarged by a sluggish surface reconstruction of the electrode[25] from ($\sqrt{3}\times23$) to (1×1) in positive potential step direction around –0.2 V. The potential range of the remarkable hysteresis roughly accords with the region of the occurrence of surface reconstruction at the negative potential than pzc. This surface reconstruction has a longer relaxation time than 10 s so that the potential scan at 10 mV/s cannot realize an equilibrium state. The atomic-level reconstruction structure of the electrode surfaces resulting in the hysteresis also depends on whether the potential was scanned to negative or positive direction.

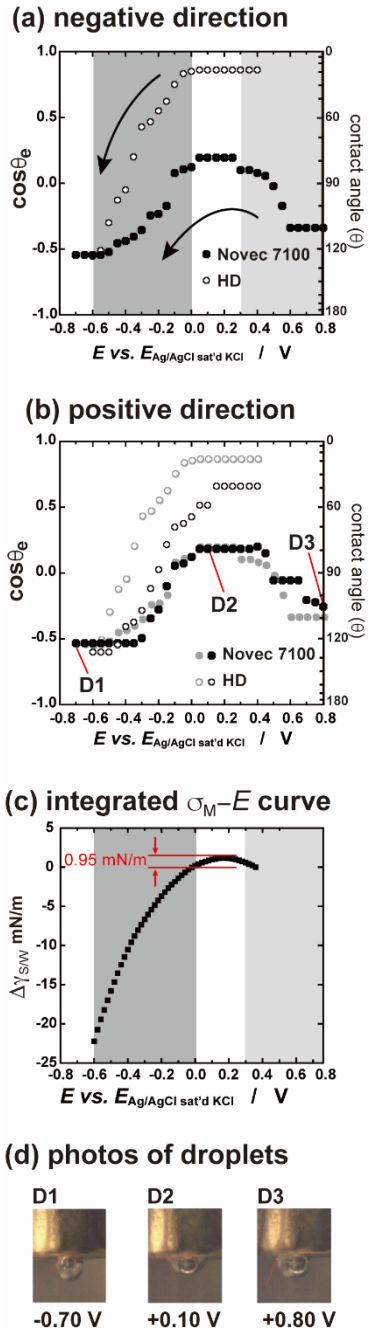

Figure 5. (a) $\cos\theta_e$–E plots obtained by potential step in negative direction for a Au(1 1 1) electrode with a Novec 1.0 μL Droplet (close circles) and a HD 1.0 μL droplet (open circles) in 50 mM $KClO_4$ solution. (b) $\cos\theta_e$–E plots obtained by potential step in positive direction (black circles) with an underlayer $\cos\theta_e$–E plot in negative direction (gray circles) copied from panel (a). The initial potential, E_i, which is the base potential for the step train, was 0.40 V (HD) and 0.80 V (Novec) for the steps to negative-going process, whereas E_i = –0.60 V (HD) and –0.80 V (Novec) for the steps to positive-going process. (c) Theoretical $\Delta\gamma_{S/W}$–E plot calculated as same plot in Fig. 2–b. (d) Calibrated photographs of a Novec droplet at Au(1 1 1)/water interface at -0.70 V (D1), +0.10 V (D2), and +0.80 V (D3) as shown in panel (b). (In this case, the Novec droplet contained a small Ar gas bubble captured in immersion process to water, whereas it did not affect experimental results).

To suppress the contribution of kinetics to the hysteresis in Fig. 4–c, we conducted the potential step measurements of θ_e to obtain Fig. 5–a and b. The potential step approach enables us to find θ_e values of near equilibrium states at constant potentials, although the potential step direction remains as a factor. Fig. 5–a shows $\cos\theta_e$–E curve for the Novec 1.0 μL droplet on a Au(1 1 1) electrode obtained by potential step experiments in negative-going direction (closed circle). The $\cos\theta_e$–E curve for a HD droplet was superimposed as open circles. The same procedures were used to obtain the $\cos\theta_e$–E curve of the HD droplet (Fig. 3–c). Fig. 5–b shows the data in positive-going direction. For Novec, smaller hysteresis depending on the direction of the potential step was observed in the range between –0.80 V and +0.20 V in the $\cos\theta_e$–E curve (Fig. 5–a and b) than in the potential-scan $\cos\theta_e$–E curve (Fig. 4–c). The value of $\cos\theta_e$ of the Novec droplet decreased at more positive potential than pzc. The decrease even in the absence of Br^- is because of positive surface charge and more orders orientation of adsorbed water molecules. The obtained $\cos\theta_e$–E curve of the Novec droplet was likely a parabolic curve in contrast to that of a HD droplet. As mentioned above, W of a Novec droplet to the Au(1 1 1) electrode surface is smaller than that of a HD droplet at a given potential. This fact resulted in a narrower plateau region around pzc (from 0.00 V to +0.30 V). A close comparison between Fig. 5–a and c in the plateau regions of $\cos\theta_e$ revealed that the $\Delta\gamma_{S/W}$ change was less than 0.95 mN/m. This value is smaller than that observed with HD (2.6 mN/m). An additional work of 0.95 mN/m is needed for $\gamma_{S/W}$ to exceed F of a Novec droplet on Au(1 1 1) surface at +0.15 V.

Especially, a Novec droplet repelled from the Au surface at E > pzc as shown in Fig. 5–a and b. Both W and F of a droplet limited the electrowetting phenomena around pzc. The Novec droplet with a lower $\gamma_{O/W}$ produced the $\cos\theta_e$–E curve with smaller hysteresis and a narrower plateau region than that of a HD droplet. Novec has smaller F than HD and showed smaller hysteresis than HD in the potential step experiments. However, Novec showed greater hysteresis in the negative potential region in the potential sweep experiment. Generally speaking, potential sweep enhances hysteresis, making the evaluation of the effect of F difficult. The reason remains unresolved.

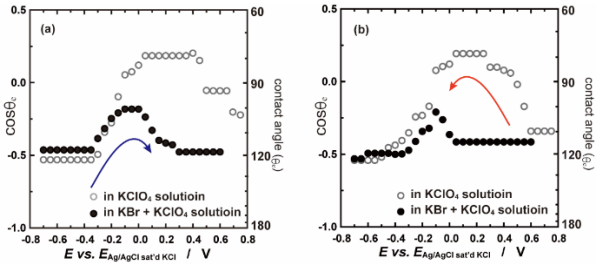

Figure 6. (a) $\cos\theta_e$–E curve obtained by potential step for a Au(1 1 1) electrode with a Novec 1.0 μL droplet in 50 mM $KClO_4$ solution (opened circles) and in 5.0 mM KBr + 50 mM $KClO_4$ solution (closed circles) in positive-going process. (b) $\cos\theta_e$–E curve of a Novec 1.0 μL droplet with (closed circles) and without KBr solution (opened circles) in negative-going process. The initial potential, E_i, which is the base potential for the step train, was –0.70 V for the steps to positive-going process, whereas E_i =+ 0.60 V (with KBr) and E_i = +0.80 V (without KBr) for the steps to negative-going process.

The effect of the specific adsorption of anion on $\cos\theta_e$ of a low-F oil droplet has never been investigated. On the other hand, the remarkable effect of the presence of Br^- on the $\cos\theta_e$–E curve of HD was demonstrated in Fig. 3. To highlight the effect on Novec, using the same concentration of KBr (5.0 mM) as in Fig. 3 in 50 mM $KClO_4$ aqueous solution, $\cos\theta_e$–E relationship for a Novec 1.0 μL droplet on a Au(1 1 1) electrode surface was plotted in Fig. 6 and compared to that without KBr. The $\cos\theta_e$–E curves were obtained by potential step for a Au(1 1 1) electrode with a Novec 1.0 μL droplet in $KClO_4$ solution (opened circles) and KBr + $KClO_4$ solution (closed circles). In the presence of Br^-, the maximum values of $\cos\theta_e$ appeared at -0.05 V in positive direction step and –0.10 V in negative direction step. The potentials of maximum $\cos\theta_e$ shifted to negative potential from that in the absence of Br^-. The values of $\cos\theta_e$ at the more positive potentials than the maximum were smaller than those without Br^-. These results showed that $\gamma_{S/W}$ decreases because of the specific adsorption of Br^- on S/W interface so that the droplet repels from the S/W interface in positive potential region. Plateau regions appeared at +0.30 V< E < +0.60 V (in positive direction step) and 0.00 V< E < +0.60 V (in negative direction step). When $\cos\theta_e$ reached to –0.5, it did not change. In this potential region, the change of $\gamma_{S/W}$ is so small that the droplet did not change its shape. The obtained $\cos\theta_e$–E curve of a Novec droplet with smaller W than that of HD to Au(1 1 1) electrode was in line with a parabolic electrocapillary curve. In contrast to a HD droplet, we found disappearance of the plateau region near pzc and expansion of the flat region over 0.3 V for a Novec droplet at the same level of $\cos\theta_e$ as in the negative potentials.

CONCLUSIONS

The electrowetting of a hydrofluoroester solvent Novec of a low $\gamma_{O/W}$ was examined as a droplet on a Au(1 1 1) electrode. The adhesion energy W and the static friction energy F as a factor to limit the electrowetting are smaller with lower $\gamma_{O/W}$. Because of smaller W with Novec, the plateau potential region, in which θ_e does not change around pzc, is narrower than that of a HD droplet. Combined use of the $\Delta\gamma_{S/W}$–E curve obtained from experimental σ_M–E curve and the experimental contact angle as a function of E enabled us to obtain F = 2.6 mN/m for HD and F = 0.95 mN/m for Novec. Because of smaller F, the value of θ_e of a Novec droplet increased at more positive potential than pzc even in the absence of specifically adsorbed Br^-. Therefore, a choice of a low $\gamma_{O/W}$ liquid should be considered to have plateau-less EWOC that can be smoothly controlled by the electrode potential. This work has left two important questions to be answered: i) why the potential sweep really enhances the hysteresis compared to the potential step, and ii) why the amplitude of the θ_e-change of Novec is smaller than that of HD. We are currently under further study.

ASSOCIATED CONTENT

The Supporting Information is available free of charge at XXXXX

Figure S1: Schematic image of contact angle measurements (PDF)

AUTHOR INFORMATION

Corresponding Author

Takamasa Sagara - Division of Chemistry and Materials Science, Graduate School of Engineering, Nagasaki University, Bunkyo 1-14, Nagasaki 852-8521, Japan; orcid.org/0000-0002-7975-394X; Email: sagara@nagasaki-u.ac.jp

Present Addresses

Tetsuro Morooka - Department of Chemistry & Life Science, Yokohama National University, 79-5 Tokiwadai, Hodogaya-ku, Yokohama, 240-8501, Japan; orcid.org/0000-0003-3436-7030; Email: morooka-tetsuro-vn@ynu.ac.jp

Author Contributions

The manuscript was written thorough contributions of all authors. All authors have given approval to the final version of the manuscript. All the experiments were prepared and conducted by T.M.

ACKNOWLEDGMENT

This work was supported by a Grant-in Aid for Scientific Research on Innovative Areas “Molecular Engine” (JSPS KAKENHI Grant Number JP19H05400) to TS and by JSPS Fellows (JSPS KAKENHI Grant Number JP19J11159) to TM.

REFERENCES

□1□ Young, T., An Essay on the Cohesion of Fluids, *Philos. Trans Soc. Lond.* **1805**, *95*, 65-87.

□2□ Zhao, Y.-P.; Y. Wang, Y.; Fundamentals and Applications of Electrowetting: A Critical Review, *Rev. Adhes. Adhes.* **2013**, *1*, 114-174.

□□□ Mugele, F.; Baret, J.-C.; Elecctrowetting: from basics to applications, *J. Phys. Condens. Matter* **2005**, *17*, R705–R774.

□4□ Nelson, W.; Kim. C.-J.; Droplet Actuation by Electrowetting-on-Dielectric (EWOD): A Review, *J. Adhes. Sci. Technol.* **2012**, *26*, 1747–1771.

□□□ Abbott, N. L.; Gorman, C. B.; Whitesides G. M.; Active Control of Wetting Using Applied Electrical Potentials and Self-Assembled Monolayers, *Langmuir* **1995**, *11*, 16-18.

□□□ Gorman, C. B.; Biebuyck, H. A.; Whitesides, G. M.; Control of the Shape of Liquid Lenses on a Modified Gold Surface Using an Applied Electrical Potential across a Self-Assembled Monolayer, *Langmuir* **1995**, *11*, 2242-2246.

□□□ Gallardo, B. C.; Gupta, V. K.; Eagerton, F. D.; Jong, L. I.; Craig, V. S.; Shah, R. R.; Abbott, N. L.; Electrochemical Principles for Active Control of Liquids on Submillimeter Scales, *Science* **1999**, *283*, 57-60.

□□□ Yamada, R.; Tada, H.; Manipulation of Droplets by Dynamically Controlled Wetting Gradients, *Langmuir* **2005**, *21*, 4254-4256.

□□□ Chaudhury, M. J.; Whitesides, G. M.; How to Make Water Run Uphill, *Science* **1992**, *256*, 1539-1541.

□1□□ Abbott, S.; Ralston, J.; Reynolds, G.; Hayes, R.; Reversible Wettability of Photoresponsive Pyrimidine-Coated Surfaces, *Langmuir*, **1999** *15*, 8923-8928.

□11□ Sumino, Y.; Kitahata, H.; Yoshikawa, K.; Nagayama, M.; Nomura, S. M.; Magome, N.; Mori, Y.; Chemosensitive running droplet, *Phys. Rev. E* **2005**, *72*, 041603–1–8.

□12□ Palma, C.; Deegan, R. D.; Droplet Translation Actuated by Photoelectrowetting, *Langmuir* **2018**, *34*, 3177–3185.

□1□□ Arscott, S.; Moving liquids with light: Photoelectrowetting on semiconductors, *Sci. Rep.* **2011**, *184*. 1-7.

□14□ Umapathi, U.; Chin, S.; Shin, P.; Koutentakis, D.; Ishii, H.; Scaling Electrowetting with Printed Circuit Boards for Large Area Droplet Manipulation, *MRS Adv.* **2018**, *3*, 1475–1483.

□1□□ Digilov, R.; Charge-Induced Modification of Contact Angle: The Secondary Electrocapilllary Effect, *Langmuir* **2000**, *16*, 6719–6723.

□1□□ Vallet, M.; Vallade, M.; Berge, B.; Limiting Phenomena for the Spreading of Water on Polymer Films by Electrowetting, *Eur. Phys. J. B* **1999**, *11*, 583–591.

□1□□ Mugele, F.; Herminghaus, S.; Electrostatic Stabilization of Fluid Microstructures, *Appl. Phys. Lett.* **2002**, *81*, 2303–2305.

□1□□ Quilliet, C.; Berge, B.; Electrowetting: A Recent Outbreak, *Curr. Opin. Colloid Interface Sci.* **2001**, *6*, 34–39.

□1□□ Jiang, C.; Ma, H.; Hasko, D. G.; Nathan, A.; Influence of Polarization on Contact Angle Saturation During Electrowetting, *Appl. Phys. Lett*. **2016**, *109*, 211601–1–4.

□2□□ Quinn, A.; Sedev, R.; Ralston, J.; Influence of the Electrical Double Layer in Electrowetting, *J. Phys. Chem. B* **2003**, *107*, 1163–1169.

□21□ Batemi, A.; Laughton, S.; Tavana, H.; Susnar, S. S.; Amirfazli, A.; Neumann, A. W.; Effect of Electric Fields on Contact Angle and Surface Tension of Drops, *J. Colloid Interface Sci.* **2005**, *283*, 215–222.

□22□ Nagai, T.; Nakanishi, S.; Nakato, Y.; Water Molecules Adsorbed at Electrode Surface Determine the Macroscopic Contact Angles, *ChemPhysChem* **2007**, *8*, 1016–1018.

□2□□ Zhang, G.; Walker, M.; Unwin, P. R.; Low-Voltage Voltammetric Electrowetting of Graphite Surfaces by Ion Intercalation/Deintercalation, *Langmuir* **2016**, *32*, 7476–7484.

□24□ Mertens, S. F. L.; Hemmi, A.; Muff, S.; Grönig, O.; De Feyter, S.; Osterwalder, J.; Greber, T.; Switching Stiction and Adhesion of a Liquid on a Solid, *Nature* **2016**, *534*, 676–679.

□2□□ Morooka, T.; Tahara, H.; Sagara, T.; Effect of bromide adsorption on electrowetting of Au electrode with hexadecane, *Electrochim. Acta* **2017**, *251*, 355–362.

□2□□ Mukouyama, Y.; Shiono, T.; Spontaneous Motion of Nitorobenzene Droplet on Au Electrode during Sn Electrodeposition, *J. Electrochem. Soc.* **2016**, *163*, H36–H41.

□2□□ Arscott, S.; Dynamic Chemically Driven Dewetting, Spreading, and Self-Running of Sessile Droplets on Crystalline Silicon, *Langmuir* **2016**, *32*, 12611–12622.

□2□□ Kornyshev, A. A.; Kucernak, A. R.; Marinescu, M.; Monroe, C. W.; Sleightholme, A. E. S.; Urbakh, M.; Ultra-Low-Voltage Electrowetting, *J. Phys. Chem. C* **2010**, *114*, 14885–14890.

□2□□ Bonn, D.; Eggers, J.; Indekeu, J.; Meunier, J.; Rolley, E.; Wetting and Spreading, *Rev. Mod. Phys.* **2009**, *81*, 739–805.

□□□□https://multimedia.3m.com/mws/media/989149O/ems-235.pdf

□□1□ Hamelin, A.; Cyclic voltammetry at gold single-crystal surfaces. Part 1. Behaviour at low-index faces, *J. Electroanal. Chem.* **1996**, *407*, 1–11.

□□2□ Jasper J.J.; Kerr E.R.; Gregorich F.; The orthobaric surface tensions and thermodynamic properties of the liquid surfaces of the n-alkanes, C5 to C18, *J. Am. Chem. Soc.* **1953**, *75*, 5252–5254.

□□□□Johnson Jr, R. E.; Dettre, R. H.; The wettability of low-energy liquid surfaces, *J. Colloid Interface Sci.* **1966**, *21*, 610–622.

□□4□ Sondag-Huethorst, J. A. M.; Fokkink, L. G. J.; Electrical double layers on thiol-modified polycrystalline gold electrodes, *J. Electroanal. Chem.* **1994**, *367*, 49–57.

□□□□Ivošević, N.; Žutić, V.; Spreading and Detachment of Organic Droplets at an Electrified Interface, *Langmuir* **1998**, *14*, 231–234.

□□□□EL-Genk, M.S.; Bostanci, H.; Saturation boiling of HFE-7100 from a copper surface, simulating a microelectronic chip, *Int. J. Heat Mass Transf.* **2003**, *46*, 1841–1854.

□□□□Lipkowski, J.; Stolberg, L.; Molecular adsorption at gold and silver electrodes, Chap. 4, in: Lipkowski, J.; Ross, P.N.; (Eds.), *Adsorption of Molecules at Metal Electrodes*, VCH, N.Y. **1992**, pp. 171–238.

□□□□de Gennes, P. G.; Wetting: statics and dynamics, *Rev. Mod. Phys.* **1985**, *57*, 827–863.

□□□□Korzeniewski, C.; Climent, V.; Feliu, J. M.; Electrochemistry at platinum single crystal electrodes, in: Bard, A. J.; Zoski C.; (Eds.), *Electroanalytical chemistry: a series of advances*, **2011**, *Vol. 24*, Ch. 2 CRC Press, 75–170.

Authors are required to submit a graphic entry for the Table of Contents (TOC) that, in conjunction with the manuscript title, should give the reader a representative idea of one of the following: A key structure, reaction, equation, concept, or theorem, etc., that is discussed in the manuscript. Consult the journal's Instructions for Authors for TOC graphic specifications.

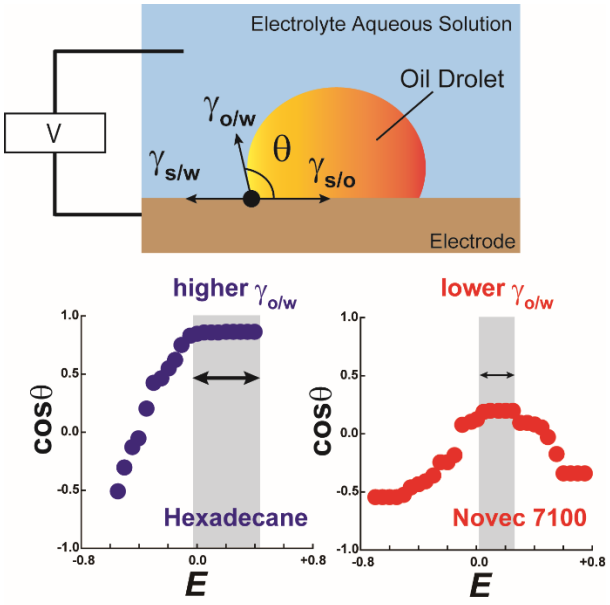

Supporting Information

Electrowetting of Hydrofluoroether Liquid Droplet at Gold Electrode/Water Interface: Significance of Lower Adhesion Energy and Static Friction Energy

Tetsuro Morooka† , Takamasa Sagara‡,*

†*Department of Advanced Technology and Science for Sustainable Development, Graduate School of Engineering, Nagasaki University, Bunkyo 1-14, Nagasaki 852-8521, Japan* and *Department of Chemistry & Life Science, Yokohama National University, 79-5 Tokiwadai, Hodogaya-ku, Yokohama, 240-8501, Japan*

‡*Division of Chemistry and Materials Science, Graduate School of Engineering, Nagasaki University, Bunkyo 1-14, Nagasaki 852-8521, Japan*

Corresponding Author: Takamasa Sagara (E-mail: sagara@nagasaki-u.ac.jp)

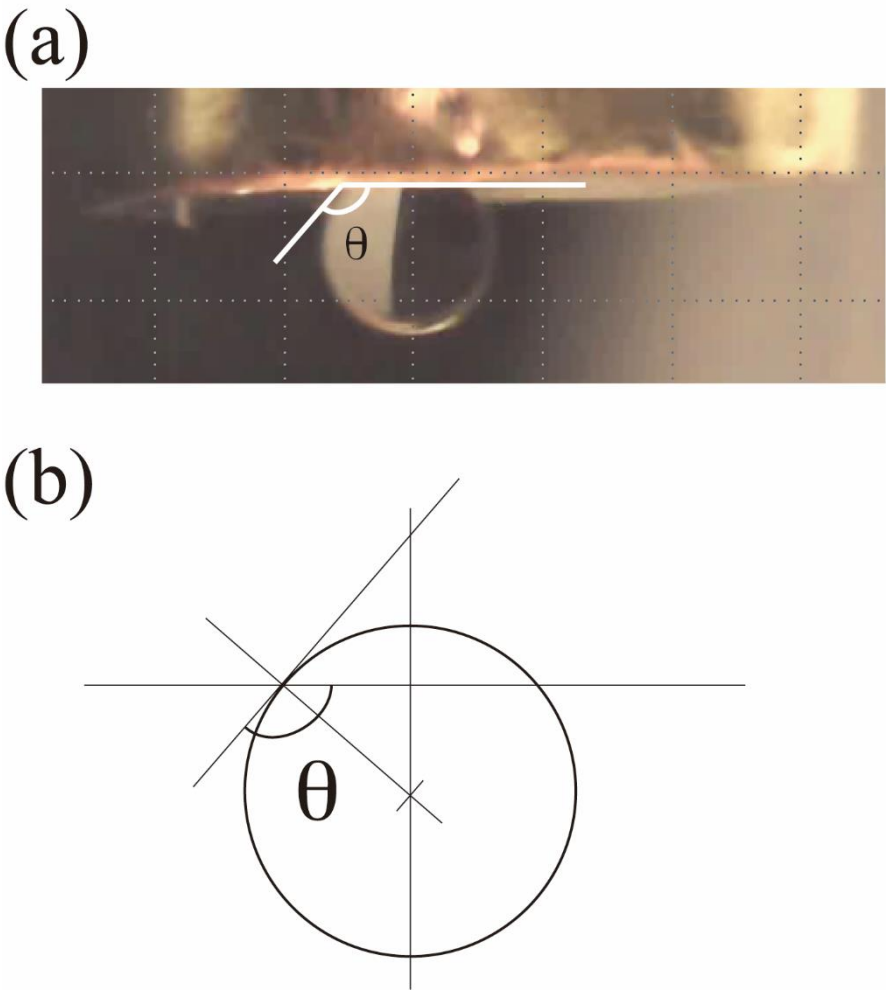

Figure S1. Photograph of the droplet at the electrode/water interface and the schematic image of measuring the contact angle of the droplet. (a) Compressed image in horizontal length by ×0.78. (b) Schematic image to measure the contact angle, θ.